Assessment of sensitivity, resolution and uncertainty in multi-dimensional electrical impedance tomography (EIT)

Work package 2
Deliverable 2.1.2

Roland Martin, Andreas Kemna

University of Bonn **(UBO)**

November 2011

Introduction

In the last two decades, electrical imaging has become a widely used exploration tool in the field of geophysics (see, e.g., Binley & Kemna [2005]). However, to date there is only a limited number of studies addressing image appraisal based on parameter uncertainty computation in electrical imaging, although this is considered essential especially for quantitative imaging applications. The understanding of the propagation of data errors and of uncertainties associated with the regularization constraint into the geophysical image represents an essential prerequisite for using the imaging results in an integrated data fusion approach aiming at parameter uncertainty prediction and risk assessment (input to WP3 and WP8).

In order to assess the characterization capabilities of the method for the present purpose, sensitivity, resolution and uncertainty in terms of parameters describing the geophysical signatures have been analyzed on the basis of already existing EIT codes. Besides the theoretical framework of Tarantola [1987], an important contribution on the latter subject was made by Alumbaugh [2000] and Alumbaugh & Newman [2000], who discussed parameter uncertainty estimation for the related electromagnetic imaging problem.

We compare qualitative and quantitative means for image appraisal by comparing coverage and resolution for a given synthetic model case and analyze the impact of varying regularization identified with a priori covariance information. Moreover, we compare, based on linearized computation schemes, parameter variance related on one hand to data errors, and on the other hand, to uncertainty in the prior model, which is typically incorporated in electrical imaging given the ill-posedness of the problem. This major difference is often overlooked, and in many works either one or the other, or even both are used for image appraisal (e.g., Oldenburg & Li [2005]) without pointing out the discrepancy. In addition, we indicate the limitation of the linearized computation approach by means of independently performed Monte-Carlo simulations which take the full non-linear character of the problem into account.

Reference model

To demonstrate the propagation of data error uncertainty and resolution measures within the optimization process and to analyze the characterization capabilities of the EIT method, we adopt a simple resistivity model which we may call a canonical EIT model. Figure 1 displays the canonical model which consists of an anomalous resistive body embedded in a homogenous background. Electrodes are placed on top and within the model domain to mimic a typical cross-borehole geometry. A typical data acquisition scheme is adopted using dipole-dipole configuration. The additional surface electrodes increase the data quality for the surface near region.

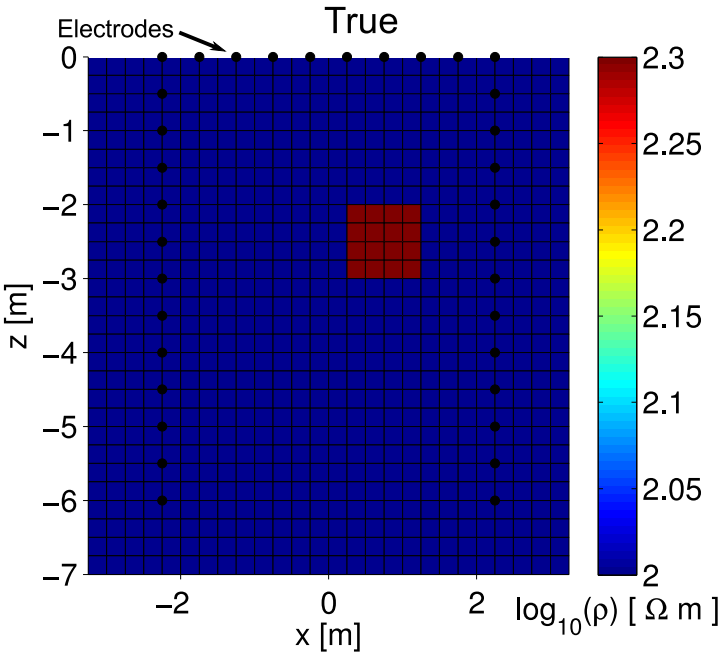

Figure 1: Exemplary resistivity model and cross borehole measurement geometry. A small resistive anomaly (contrast 2:1) is embedded in a homogenous 100 Ωm background. Electrodes are marked with black dots. The whole measurement geometry consists of 34 electrodes placed at .5 m distance assuming a "skip-one" dipole-dipole measurement protocol [Slater et al., 2000] 334 times. The investigated area covers a dimension of $6.5 \times 7\,\mathrm{m}^2$ and is uniformly discretized into 783 quadratic cells of .25 m edge length.

Optimal model parameter estimation

The non-linear inverse problem in electrical impedance tomography, i.e., the optimal estimation of M complex model parameters $\boldsymbol{m}^* \in \mathbb{C}^M$ from N given measured (complex) data $\boldsymbol{d} \in \mathbb{C}^N$, contaminated by noise, is usually solved in a deterministic way by solving the normal equations of the linearized and regularized [Tikhonov & Arsenin, 1977] problem for the n'th model update $\delta\boldsymbol{m}_n$, starting at the prior guess $\boldsymbol{m}_{m0}$,

$$\left(\mathbf{A}_n^{\mathsf{H}}\mathbf{C}_d^{-1}\mathbf{A}_n + \lambda\mathbf{R}^{\mathsf{T}}\mathbf{R}\right)\delta\boldsymbol{m}_n = \left(\mathbf{A}_n^{\mathsf{H}}\mathbf{C}_d^{-1}\left(\boldsymbol{d} - \boldsymbol{f}(\boldsymbol{m}_n)\right) - \lambda\mathbf{R}^{\mathsf{T}}\mathbf{R}\left(\boldsymbol{m}_n - \boldsymbol{m}_{m0}\right)\right)\,, \qquad (1)$$

and forming a converging sequence to determine the optimal estimate (OE) after n^* iterations:

$$\boldsymbol{m}^* = \boldsymbol{m}_{m0} + \sum_n^{n^*} \alpha_n \delta\boldsymbol{m}_n\,. \qquad (2)$$

Here, $\boldsymbol{f}$ describes the non linear model response which maps parameter space into data space: $\left(\boldsymbol{f}(\boldsymbol{m}) : \mathbb{C}^M \to \mathbb{C}^N\right)$. $\mathbf{A}$ is the Jacobian matrix of partial derivatives (i.e. $A_{ij} := \partial f_i(\boldsymbol{m})/\partial m_j$) displaying the sensitivity of the i'th forward model prediction with respect to changes of the j'th model parameter m_j, $\mathbf{C}_d$ the data covariance matrix, which is a diagonal matrix for uncorrelated data errors (i.e. $\mathbf{C}_d = \{\epsilon_{ii}^2\}$), $\mathbf{R}$ the roughness matrix imposing a smoothness constraint on the model (regularization), λ the regularization parameter, and

$0 < \alpha \leq 1$ is the step length of each model update[1]. $^{\mathsf{H}}$ denotes the conjugate transpose operator.

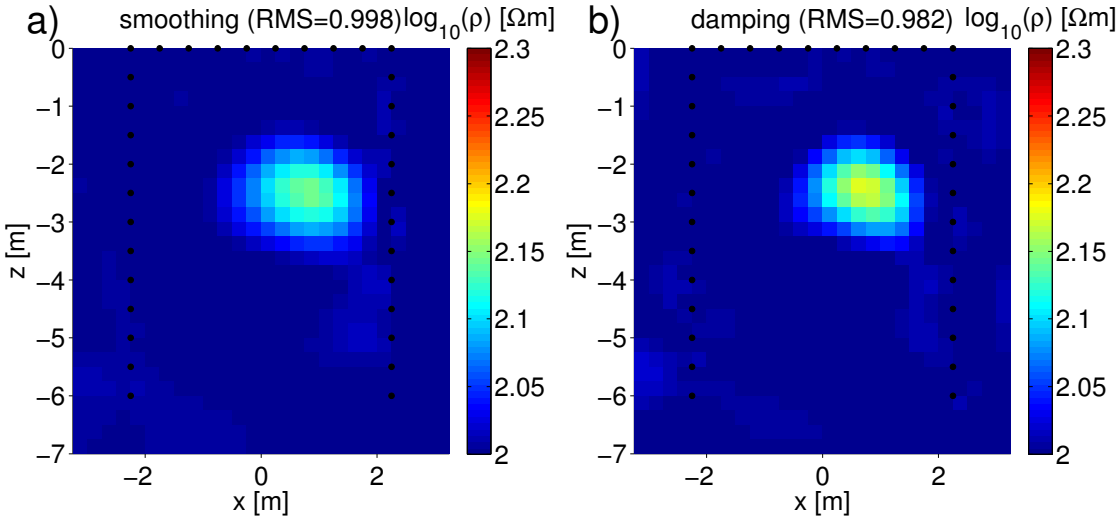

Figure 2: Smoothed (OCCAM-OE) (a) and damped (Marquardt-OE) (b) optimal estimates for the resistivity value (log magnitude). The regularization parameter was chosen via one dimensional line search subject to fit the data as good as possible.

To demonstrate the impact of different regularization strategies, we computed the optimal estimation of the reference model (Fig. 1), with two different regularization strategies. The smooth model, OCCAM inversion [Constable et al., 1987], maintains active regularization between neighboring model cells via a discretized first-order finite-difference operator matrix as outlined in [Kemna, 2000]. In contrast, a pure damping approach uses $\mathbf{R}^{\mathsf{T}}\mathbf{R} \equiv \mathbf{I}$ as regularization, which is also known as Marquardt damping [Marquardt, 1963]. Here, the regularization parameter is sought of as a damping parameter, stabilizing vanishing entries in $\mathbf{A}^{\mathsf{H}}\mathbf{C}_d^{-1}\mathbf{A}$, but without taking cell connection into account. As can be seen from Figure 2a, the smooth inversion favors interconnected model estimates, whereas the Marquardt-damping (Fig. 2b), although the Marquardt-OE possesses the same data fit, tends to incorporate more structure within the inversion process. However, both regularization strategies results in reasonable reconstruction of the resistive anomaly.

Complex data and model parameter representation

Within the optimal estimation, log transformed parameters and data are used to account for the wide dynamic range of conductivity magnitudes for earth materials. The model vector $\boldsymbol{m}$ and data vector $\boldsymbol{d}$ are defined as

$$m_j := \ln \rho_j = \ln |\rho_j| + \mathrm{i}\varphi_j, \quad (j = 1, \ldots, M)\,, \tag{3}$$

$$d_i := \ln Z_i = \ln |Z_i| + \mathrm{i}\varphi_i, \quad (i = 1, \ldots, N)\,, \tag{4}$$

[1]usually $\alpha \approx 1$, but it can be optimized in a last parabola fitting routine [Kemna, 2000] as well.

where

$$\rho_j = |\rho_j| \, e^{\mathrm{i}\varphi_j} \tag{5}$$

are the complex resistivities discretized on a finite element mesh,

$$Z_i = \frac{V_i}{I_i} = |Z_i| e^{\mathrm{i}\varphi_i} \tag{6}$$

are the measured complex transfer impedances with $\mathfrak{i}^2 = -1$. Note, that the complex log function in equations (3) and (4) separates the log magnitude and phase of its argument into real and imaginary part, for example $\mathfrak{Re}(d) = \ln |Z|$ and $\mathfrak{Im}(d) = \varphi$.

From the equations (3) and (4) follows, that the elements of the Jacobian matrix are altered as well. By applying the complex version of the chain rule, the complex valued sensitivity is computed like

$$A_{ij} = \frac{\partial f_i(\boldsymbol{m})}{\partial m_j} \begin{array}{c} (I_i = 1) \\ = \end{array} \frac{\rho_j}{V_i} \frac{\partial V_i}{\partial \rho_j} \tag{7}$$

The right-hand side of equation (7) is computed via the superposition of adjoint fields (e.g. Kemna [2000]).

Although for real valued problems, the data can vary only in one dimension, i.e., any data noise is one-dimensional, a complex number may be subject to errors in two dimensions if the real and imaginary parts yield stochastically independent random variables. To describe the misfit of the complex quantities, we express the denominators of the chi-squared data misfit functional according to [Kemna, 2000]:

$$\psi_d(\boldsymbol{m}) = [\boldsymbol{d} - \boldsymbol{f}(\boldsymbol{m})]^{\mathsf{H}} \, \mathbf{C}_d^{-1} \, [\boldsymbol{d} - \boldsymbol{f}(\boldsymbol{m})] \tag{8}$$

$$= \sum_i \frac{|d_i - f_i(\boldsymbol{m})|^2}{|\epsilon_i|^2} \,, \tag{9}$$

with

$$\epsilon_i = s(\ln |Z_i|) + \mathfrak{i} s(\varphi_i) \,, \tag{10}$$

where $s()$ denotes the standard deviation of the quantity. These values may be determined from reciprocal analysis (i.e. Flores Orozco et al. [2011]; Slater et al. [2000]), by statistical means or estimated according to numerical considerations (electrode spacing, mesh quality, etc.).

Image appraisal estimations

In this work we consider three approaches to evaluate our optimal estimation:

1. The sensitivity or accumulated sensitivity,

2. the resolution matrix and

3. the posteriori covariance matrix.

We compare their individual results under qualitative and quantitative aspects.

Sensitivity (accumulated sensitivity)

To investigate the sensitivity becomes plausible from its genesis: In most deterministic imaging framework it is the driver of the whole iterative process and therefore, besides data covariance, controls most of the data driven part within posteriori model estimation. Secondly, it is computationally inexpensive to compute and therefore one of the first choices for the qualitative appraisal of the OE.

The sensitivity, or Frechét derivative, is defined as mapping the small changes of the forward model with respect to small changes in model space. The idea of the accumulated sensitivity is, instead of examining every entry of the Jacobian matrix, which will be to complex to investigate for large data sets, to compute the absolute influence of one parameter change to the complete data set, i.e. to map how specific regions of the model space are "covered" by the data. Thus the synonym coverage is also applied for the sensitivity. Yet, we favor the second name because of it's inherent link to the 'real" sensitivity entries of the Jacobian matrix.

Analogous to seismic tomography, where ray coverage is given by the sum of the respective ray segments in each model cell, we compute the sensitivity as

$$\mathrm{c}_j = \sum_i^N |A_{ij}| \tag{11}$$

or, if we take the data covariance into account as

$$\mathrm{c}_j^d = \sum_i^N \frac{|A_{ij}|^2}{|\epsilon_i|^2} = \left(\mathbf{A}^{\mathsf{H}}\mathbf{C}_d^{-1}\mathbf{A}\right)_{jj} , \tag{12}$$

which represents exactly the diagonal entries of our Hessian approximation within OE, except that the sensitivity is computed for the optimal model after the iterative process (eq. 2) terminates.

Obviously, a poorly covered region is unlikely to be well resolved and thus, the sensitivity may give some crude indication for how well the model parameter is represented by the data set. However, it must be emphasized, that high sensitivity does not necessary imply high resolution but rather represents a favoring factor.

Resolution matrix

In contrast to the crude, but easy to compute estimation of resolution via equation (12), the posteriori resolution matrix, as used in classic inversion theory (e.g. [Menke, 1984]), addresses the question if all model parameters are independently resolved or not (with emphasize on their independence).

Resolution of linear inversion

To explore this question we first reconsider the linear case and imagine that there is a true, but unknown set of model parameters $\boldsymbol{m}^{**}$ such that the data are equated by a kernel matrix $\mathbf{G}$ with the true model (i.e. $\mathbf{G} \equiv \mathbf{A}$):

$$\boldsymbol{d} = \mathbf{G}\boldsymbol{m}^{**} \,. \tag{13}$$

The inverse process defines a generalized inverse $\mathbf{G}^{\dagger} = \left(\mathbf{G}^{\mathsf{H}}\mathbf{G}\right)^{-1}\mathbf{G}$ (Moore-Penrose-inverse) used to find the model estimate

$$\boldsymbol{m}^{*} = \mathbf{G}^{\dagger}\boldsymbol{d}\,. \tag{14}$$

Combining equation (13) with (14) yields

$$\boldsymbol{m}^{*} = \mathbf{G}^{\dagger}\mathbf{G}\boldsymbol{m}^{**} = \mathbf{R}^{\mathsf{M}}\boldsymbol{m}^{**}\,. \tag{15}$$

The real valued square matrix $\mathbf{R}^{\mathsf{M}} = \mathbf{G}^{\dagger}\mathbf{G}$ combines forward and inverse mapping and is referred to as resolution matrix.

Non linear resolution

For non linear inversion, we consider the case, where the data vector is ideally mapped via the forward operator of the true model, i.e. $\boldsymbol{d} = \boldsymbol{f}\left(\boldsymbol{m}^{**}\right)$. We now want to find the expression how good this assumption is represented by the actual model estimate.

We start our investigations with a Taylor series around the n^{*}'th model estimate:

$$\boldsymbol{d} = \boldsymbol{f}(\boldsymbol{m}^{**}) = \boldsymbol{f}\left(\boldsymbol{m}_{n^{*}}\right) + \mathbf{A}_{n^{*}}\left(\boldsymbol{m}^{**} - \boldsymbol{m}_{n^{*}}\right) + \mathcal{O}\left(\boldsymbol{m}^{**} - \boldsymbol{m}_{n^{*}}\right)^{2} \,. \tag{16}$$

Let us now assume, that the model estimate is already close to the true model. That means that higher order terms ($\mathcal{O}((\boldsymbol{m}^{**} - \boldsymbol{m}_{n^{*}})^{2})$) can be neglected. For simplification, we define the generalized inverse for the regularized case:

$$\mathbf{A}^{\dagger}_{n^{*}} := \left(\mathbf{A}^{\mathsf{H}}_{n^{*}}\mathbf{C}_{d}^{-1}\mathbf{A}_{n^{*}} + \lambda\mathbf{R}^{\mathsf{T}}\mathbf{R}\right)^{-1} \,. \tag{17}$$

Without loss of generality we take the next model update as our final model estimate, that is

$$\begin{aligned}\boldsymbol{m}^{*} =& \boldsymbol{m}_{n^{*}} + \delta\boldsymbol{m}_{n^{*}} \\ =& \boldsymbol{m}_{n^{*}} + \mathbf{A}^{\dagger}_{n^{*}}\left[\mathbf{A}^{\mathsf{H}}_{n^{*}}\mathbf{C}_{d}^{-1}\left(\boldsymbol{d} - \boldsymbol{f}(\boldsymbol{m}_{n^{*}})\right) - \lambda\mathbf{R}^{\mathsf{T}}\mathbf{R}\left(\boldsymbol{m}_{n^{*}} - \boldsymbol{m}_{m0}\right)\right] \,,\end{aligned} \tag{18}$$

and replace $\boldsymbol{d} - \boldsymbol{f}\left(\boldsymbol{m}_{n^{*}}\right) = \mathbf{A}_{n^{*}}\left(\boldsymbol{m}^{**} - \boldsymbol{m}_{n^{*}}\right)$ as the remainder term of equation (16) in equation (18). Thus, the last optimal estimate reads

$$\begin{aligned}\boldsymbol{m}^{*} =& \boldsymbol{m}_{n^{*}} + \mathbf{A}^{\dagger}_{n^{*}}\mathbf{A}^{\mathsf{H}}_{n^{*}}\mathbf{C}_{d}^{-1}\mathbf{A}_{n^{*}}\left(\boldsymbol{m}^{**} - \boldsymbol{m}_{n^{*}}\right) - \lambda\mathbf{A}^{\dagger}_{n^{*}}\mathbf{R}^{\mathsf{T}}\mathbf{R}\left(\boldsymbol{m}_{n^{*}} - \boldsymbol{m}_{m0}\right) \\ =& \boldsymbol{m}_{n^{*}} - \mathbf{A}^{\dagger}_{n^{*}}\mathbf{A}^{\mathsf{H}}_{n^{*}}\mathbf{C}_{d}^{-1}\mathbf{A}_{n^{*}}\boldsymbol{m}_{n^{*}} - \lambda\mathbf{A}^{\dagger}_{n^{*}}\mathbf{R}^{\mathsf{T}}\mathbf{R}\boldsymbol{m}_{n^{*}} \\ &+ \mathbf{A}^{\dagger}_{n^{*}}\mathbf{A}^{\mathsf{H}}_{n^{*}}\mathbf{C}_{d}^{-1}\mathbf{A}_{n^{*}}\boldsymbol{m}^{**} + \lambda\mathbf{A}^{\dagger}_{n^{*}}\mathbf{R}^{\mathsf{T}}\mathbf{R}\boldsymbol{m}_{m0}\,.\end{aligned} \tag{19}$$

In equation (19) we can identify

$$\mathbf{A}^\dagger \mathbf{A}^\mathsf{H} \mathbf{C}_d^{-1} \mathbf{A} + \lambda \mathbf{A}^\dagger \mathbf{R}^\mathsf{T} \mathbf{R} = \mathbf{A}^\dagger \left(\mathbf{A}^\mathsf{H} \mathbf{C}_d^{-1} \mathbf{A} + \lambda \mathbf{R}^\mathsf{T} \mathbf{R} \right) = \mathbf{I} \,, \tag{20}$$

and in the manner of the linear case, we define the non linear model resolution matrix of the n'th model iterate as

$$\mathbf{R}^\mathsf{M}_{n^*} := \mathbf{A}^\dagger_{n^*} \mathbf{A}^\mathsf{H}_{n^*} \mathbf{C}_d^{-1} \mathbf{A}_{n^*} \,. \tag{21}$$

With the identities of (20) and the definition (21) we can express the final estimate in terms of resolution matrices:

$$\boldsymbol{m}^* = \mathbf{R}^\mathsf{M}_{n^*} \boldsymbol{m}^{**} + \left(\mathbf{I} - \mathbf{R}^\mathsf{M}_{n^*} \right) \boldsymbol{m}_{m0} \,. \tag{22}$$

In practice, the resolution matrix is computed for the OE, and not for the last but one model estimate ($\mathbf{R}^\mathsf{M}_{n^*} \approx \mathbf{R}^\mathsf{M}_{m^*}$). However, in the same sense as in the linear case, the resolution matrix maps the true model into the final non linear model estimate, our OE. Yet, in contrast to the linear case, the OE is filled up with the starting model at regions of missing resolution.

Discussion

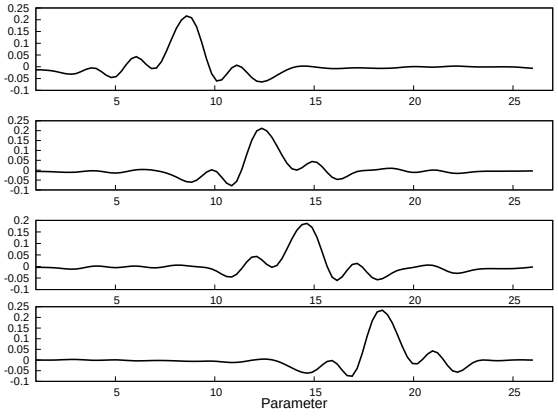

Figure 3: Exemplary entries of the non linear resolution matrix from 4 adjacent model parameters with respect to parameters at the same depth.

If $\mathbf{R}^\mathsf{M}$ equals the unity matrix each model parameter is uniquely determined. If $\mathbf{R}^\mathsf{M}$ is not the identity matrix, the estimated model parameters are averages of the true model parameters

$$m_j^* = \sum_i^M R^\mathsf{M}_{ij} m_i^{**} \,, \tag{23}$$

which basically means, that the i'th line of $\mathbf{R}^\mathsf{M}$ is the weighting function for the j'th parameter estimate. This underlying behavior is addressed by figure 3. It displays how anomalies in the corresponding model cells are mapped via the combination of measurement and inverse modeling. The entries within each line may also be sought of as spread of the resolution transferring the reality into our model and is well connected to the kernel function of Backus & Gilbert [1968]. If each entry contains a sharp delta peak at the main diagonal position, this parameter would be uniquely identified. The bigger the off diagonal entries are, the more averaging from adjacent parameters is incorporated into the OE.

Figure 4 compares data error weighted sensitivity, as defined by eq. (12) with the main diagonal entries of the non linear resolution matrix according to eq. (21). Both,

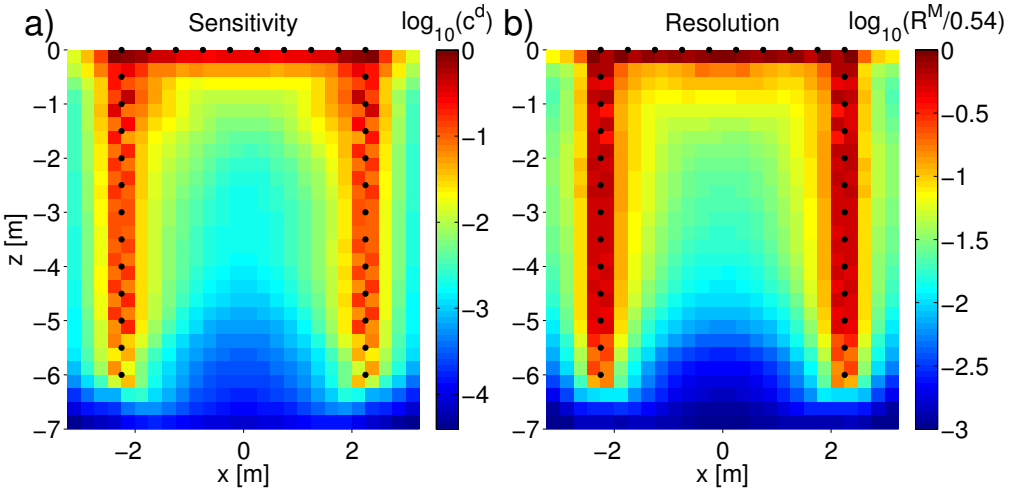

Figure 4: Exemplary calculations of weighted sensitivity according to eq. (12) (a) and main diagonal resolution matrix (b) for the OCCAM-OE (Fig. 2a). Figure a): red values correspond to sensitive areas (i.e. around the electrodes) whereas regions colored in blue (i,e, below 10^{-3}) correspond to low sensitive sub domains. Red values in Fig. (b) show comparably good resolved model parameters whereas regions of blue color are less well determined model parameters. In contrast to the sensitivity, the resolution matrix exhibit a pattern more focused on the areas around the electrodes. Also note, that no parameter is uniquely defined within the optimal estimation.

the sensitivity and the resolution matrix reveal similar patterns, expressing their inherent similarity. Yet, the non linear resolution matrix entries where computed using appropriate regularization for this particular problem, where the data driven part of the inverse solution is already good represented, i.e. the left hand side of equation (22) is comparably good conditioned.

In contrast to the similar patterns of figure 4, we can see in figure 5 how the resolution changes by varying the regularization parameter. If we compare the resolution matrix obtained with different regularization strength (fig. 5) that the resolution changes dramatically: The resolution decreases inverse proportional to increasing regularization, which is perfectly intended by it's definition. Yet, the difference in non linear resolution with varying regularization also demonstrates the main difference between qualitative appraisal of the OE due to sensitivities (fig. 4, a) compared to quantitative EIT evaluation (figs. 4 b and 5 a,b). The

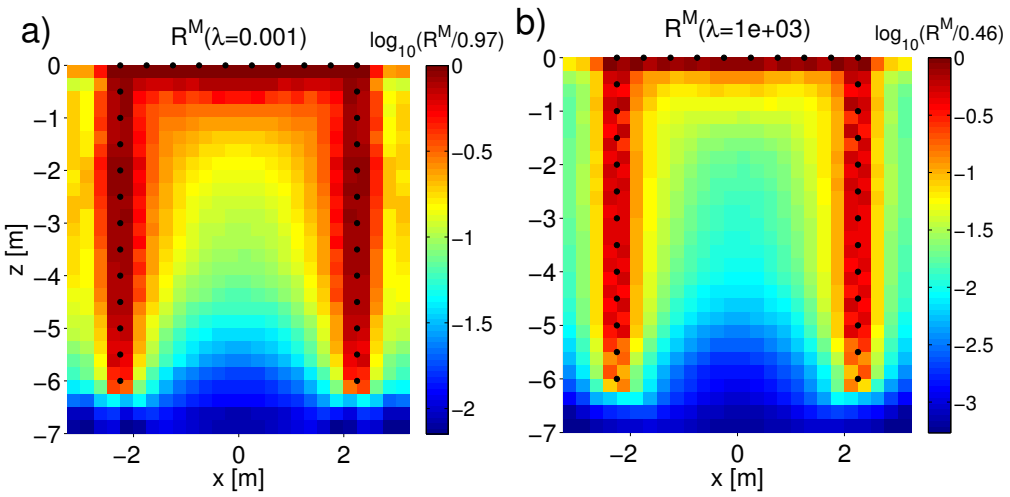

Figure 5: Exemplary calculation main diagonal resolution matrix for the OCCAM-OE (Fig. 2a), using smooth regularization with small regularization parameter (a) and for very strong regularization (b).

A posteriori covariance calculation

Linear model uncertainty computation

Following Tarantola [1987], the a posteriori model covariance matrix $\mathbf{C}_{m^*}$, describing the covariance of the OE given the prior model covariance matrix $\mathbf{C}_{m0}$, is given by

$$\mathbf{C}_{m^*} = \left(\mathbf{A}_{m^*}^{\mathsf{H}} \mathbf{C}_d^{-1} \mathbf{A}_{m^*} + \mathbf{C}_{m0}^{-1}\right)^{-1} . \tag{24}$$

If we identify the regularization term in equation (1) with the inverse prior model covariance matrix (i.e., considering λ as an inverse measure of model variance magnitude, see for instance Alumbaugh [2000]), the posteriori model covariance can be computed according to

$$\mathbf{C}_{m^*}^{m}(\lambda) = \left(\mathbf{A}_{m^*}^{\mathsf{H}} \mathbf{C}_d^{-1} \mathbf{A}_{m^*} + \lambda \mathbf{R}^{\mathsf{T}} \mathbf{R}\right)^{-1} . \tag{25}$$

In contrast to equation (25), a model covariance matrix of the estimated parameters associated with data errors can be computed from equation (1) following the rules of error propagation (e.g., Gubbins [2004]):

$$\mathbf{C}_{m^*}^{d}(\lambda) = \left(\mathbf{A}_{m^*}^{\mathsf{H}} \mathbf{C}_d^{-1} \mathbf{A}_{m^*} + \lambda \mathbf{R}^{\mathsf{T}} \mathbf{R}\right)^{-1} \mathbf{A}_{m^*}^{\mathsf{H}} \mathbf{C}_d^{-1} \mathbf{A}_{m^*} \left(\mathbf{A}_{m^*}^{\mathsf{H}} \mathbf{C}_d^{-1} \mathbf{A}_{m^*} + \lambda \mathbf{R}^{\mathsf{T}} \mathbf{R}\right)^{-1} . \tag{26}$$

Non linear model uncertainty computation (Monte Carlo approach)

Tarantola [1987] recommends to estimate the full non-linear a posteriori model covariance matrix via a Monte Carlo approach. This involves running the full non-linear inversion, say $K^d \times K^m$ times, with each time adding numbers from a separate Gaussian random ensemble with zero mean to the prior model and the data, respectively. Computing this,

results in the K^d-fold estimates

$$\boldsymbol{m}_k^{m^*}(\sigma^m) = \boldsymbol{m}_{m0} + \sum_n \alpha_n \left(\mathbf{A}_n^{\mathsf{H}}\mathbf{C}_d^{-1}\mathbf{A}_n + \lambda_n\mathbf{R}^{\mathsf{T}}\mathbf{R}\right)^{-1}\left[\mathbf{A}_n^{\mathsf{H}}\mathbf{C}_d^{-1}\left(\boldsymbol{d} - \boldsymbol{f}(\boldsymbol{m}_n)\right)\right. \\ \left. -\lambda\mathbf{R}^{\mathsf{T}}\mathbf{R}\left(\boldsymbol{m}_n - \boldsymbol{m}_{m0} + \boldsymbol{r}_k^m(\sigma^m)\right)\right], \quad (k = 1, \ldots, K^m), \tag{27}$$

to compute the uncertainty due to a priori errors (equivalent to eq. (25)), and

$$\boldsymbol{m}_k^{d^*}(\sigma^d) = \boldsymbol{m}_{m0} + \sum_n \alpha_n \left(\mathbf{A}_n^{\mathsf{H}}\mathbf{C}_d^{-1}\mathbf{A}_n + \lambda_n\mathbf{R}^{\mathsf{T}}\mathbf{R}\right)^{-1}\left[\mathbf{A}_n^{\mathsf{H}}\mathbf{C}_d^{-1}\left(\boldsymbol{d} - \boldsymbol{f}(\boldsymbol{m}_n) + \boldsymbol{r}_k^d(\sigma^d)\right)\right. \\ \left. -\lambda\mathbf{R}^{\mathsf{T}}\mathbf{R}\left(\boldsymbol{m}_n - \boldsymbol{m}_{m0}\right)\right], \quad \left(k = 1, \ldots, K^d\right), \tag{28}$$

for the uncertainty due to data errors (equivalent to eq. (26)).

Here, $\sigma^{d,m}$ denotes the (constant) variance of each Gaussian random ensemble

$$\left\{\boldsymbol{r}_k^{d,m}(\sigma) : k \in \mathbb{N},\ \sigma \in \mathbb{R}_{>0},\ \boldsymbol{r}^{d,m} \in \mathbb{R}^{N,M}\right\}, \tag{29}$$

with

$$r_{k_i}(\sigma) = \sigma x_{k_i}\sqrt{-2log(z_{k_i})/z_{k_i}}, \quad i = 1, \ldots, \{N, M\}. \tag{30}$$

In equation (30), $x_{k_i} \in [0, \ldots, 1]$ and $y_{k_i} \in [0, \ldots, 1]$ are drawn from uniform random distributions and $z_{k_i} := x_{k_i}^2 + y_{k_i}^2 > 1$. Note, that each random ensemble $\left\{\boldsymbol{r}_k^{d,m}(\sigma)\right\}$ is statistical independent from the others, i.e. the seeds used to produce the pseudo random numbers are different for each ensemble. Also note, that the variance σ^m of the random ensembles $\{\boldsymbol{r}_k^m\}$ corresponds to the uncertainty in the prior model scaled by λ.

Finally, the covariance of the non linear Monte Carlo approach reads

$$\mathbf{C}_{m^*,\mathsf{nl}}^{d,m}\left(\sigma^{m,d}\right) = \frac{1}{K-1}\sum_k^{K^{d,m}}\left(\boldsymbol{m}_k^{d^*,m^*} - \overline{\boldsymbol{m}}^{d^*,m^*}\right)^{\mathsf{H}}\left(\boldsymbol{m}_k^{d^*,m^*} - \overline{\boldsymbol{m}}^{d^*,m^*}\right) \tag{31}$$

where $\overline{\boldsymbol{m}}^{d^*,m^*} = \frac{1}{K^{d,m}}\sum_k^{K^{d,m}}\boldsymbol{m}_k^{d^*,m^*}$ is the mean model parameter of the K^d, K^m final estimates.

Discussion

To examplify the differences between linear and non-linear uncertainty calculations we inverted noise-contaminated data (5% relative resistance error) and computed uncertainty of the smooth model OE on the basis of the two different linear schemes (Figs. 7 a, b) as well as via the Monte Carlo approach (Figs. 7 c, d). From the resulting K^d and K^m inverted models the mean inverted resistivity model (not shown here) and the non-linear a posteriori model covariance (Figs. 7 c,d; Figs. 6 a,b) are computed as previously outlined.

Last not least, in figure 8 we compare the uncertainties obtained by means of different regularization strategies and regularization strength. Displayed to the left side (a-c), we

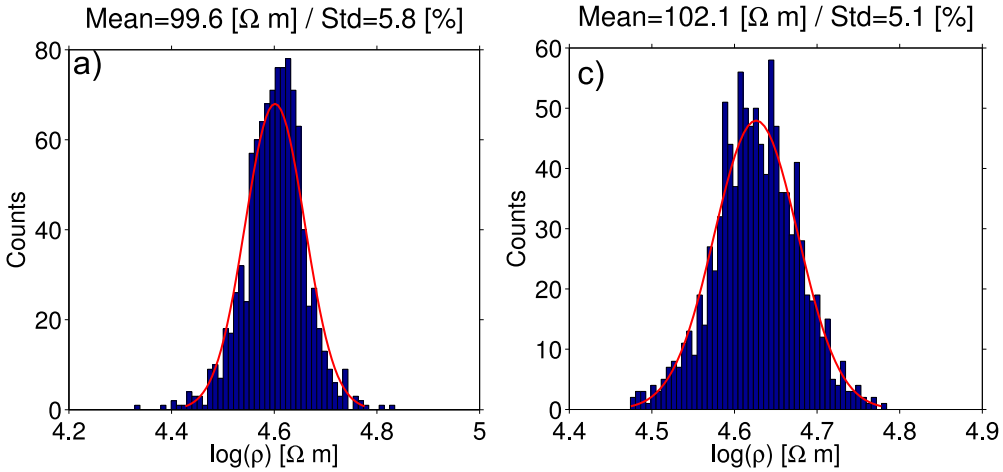

Figure 6: Histogram analysis of the Monte Carlo simulations for uncertainty calculation of the OE by statistical means. a) displays the ensemble histogram of one parameter for the Monte Carlo approach of the data error quantification and c) shows the adequate histogram statistics for the impact of random noise on the prior model.

calculated the linear posteriori uncertainty (eq. (25)) due to smooth regularization and in (d-f) we show the uncertainty of the Marquardt-OE. From top (a,d) to bottom (c,f) we increased the regularization parameter, which controls the regularization strength from very small regularization ($\lambda = 10^{-5}$, top) to very strong regularization ($\lambda = 10^{3}$, bottom).

A qualitative comparison of the uncertainty patterns obtained with different regularizations, i.e. comparing left to the right side, expresses the inherent difference between OCCAM and Marquardt regularization:

Whereas the smooth regularization obtains the biggest uncertainty in areas of no spatial regularization (i.e. the borders of the model), where there are fewer adjacent cells to constrain the value, the uncertainty pattern of the dampened OE is independent of the spatial position of the cells and only influenced by the electrode positions, i.e. highest sensitivity. If we compare the values obtained with the two different regularization strategies and small regularization, they are relatively comparable (although they are very high), expressing also the similarity in the OE (figs. 2), which yield basically the same structure. However, for $\lambda = 1$, the OCCAM inversion reproduces much less uncertainty within sensitive areas (i.e., the standard deviation is $\approx 35\%$ around the electrodes) compared to the standard deviation for Marquardt damping ($\approx 56\%$). The most extreme effect on the posteriori covariance is obtained with strong regularization, where the inverse related prior variance (i.e., the λ) controls the posteriori error. Both regularization strategies will than drop the standard deviation of the OE below 2.5% within good resolved regions. Yet, the Marquardt damping over represents the regions around the electrodes and the OCCAM regularization is more related to the general sensitivity pattern.

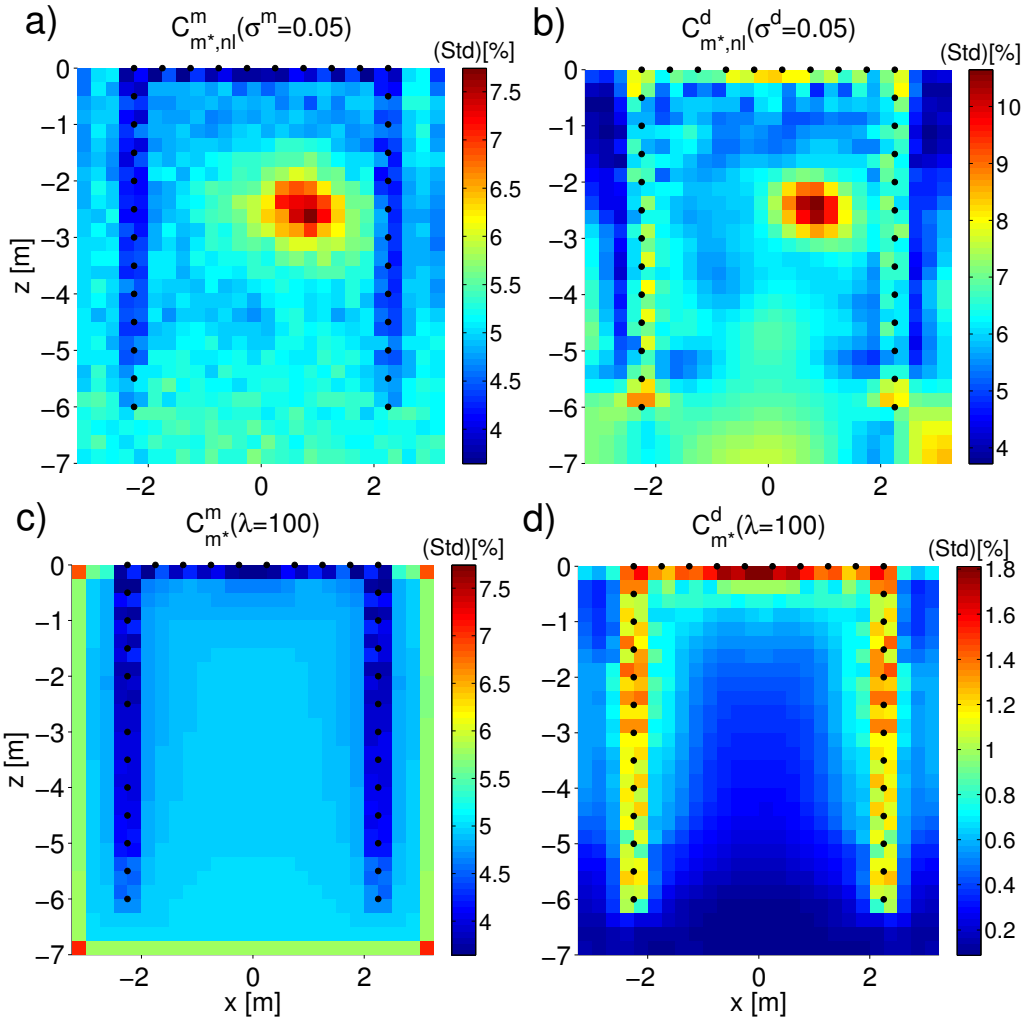

Figure 7: Results of non linear (a, b) and linear (b, c) uncertainty calculations. The results shown in a and b are the variances obtained from eq. (31) with respect to a priori noise variation (i.e. Monte Carlo simulation of eq. (27)) and with respect to data error (i.e. Monte Carlo simulation of eq. (28)). For c, we used the classical formula (eq. (25)) and within d, the impact of data error by computing eq. (26) is displayed.

Conclusions and outlook

The two linear schemes for model uncertainty computation yield different results, both qualitatively and quantitatively. Importantly, the spatial patterns are inversely related: While data errors cause higher uncertainties in well resolved areas than in regions dominated by the regularization (i.e. prior covariance), the uncertainty associated with the prior model is highest in regions which are only poorly controlled by the data. This inverse behavior, however, just reflects the different definitions of model uncertainty in the two approaches - a trivial, but yet often overlooked aspect in electrical image appraisal. The independent Monte Carlo results for data and prior model error propagation exhibit the same general patterns. Remarkably, the distributions of the individual parameter estimates ex-

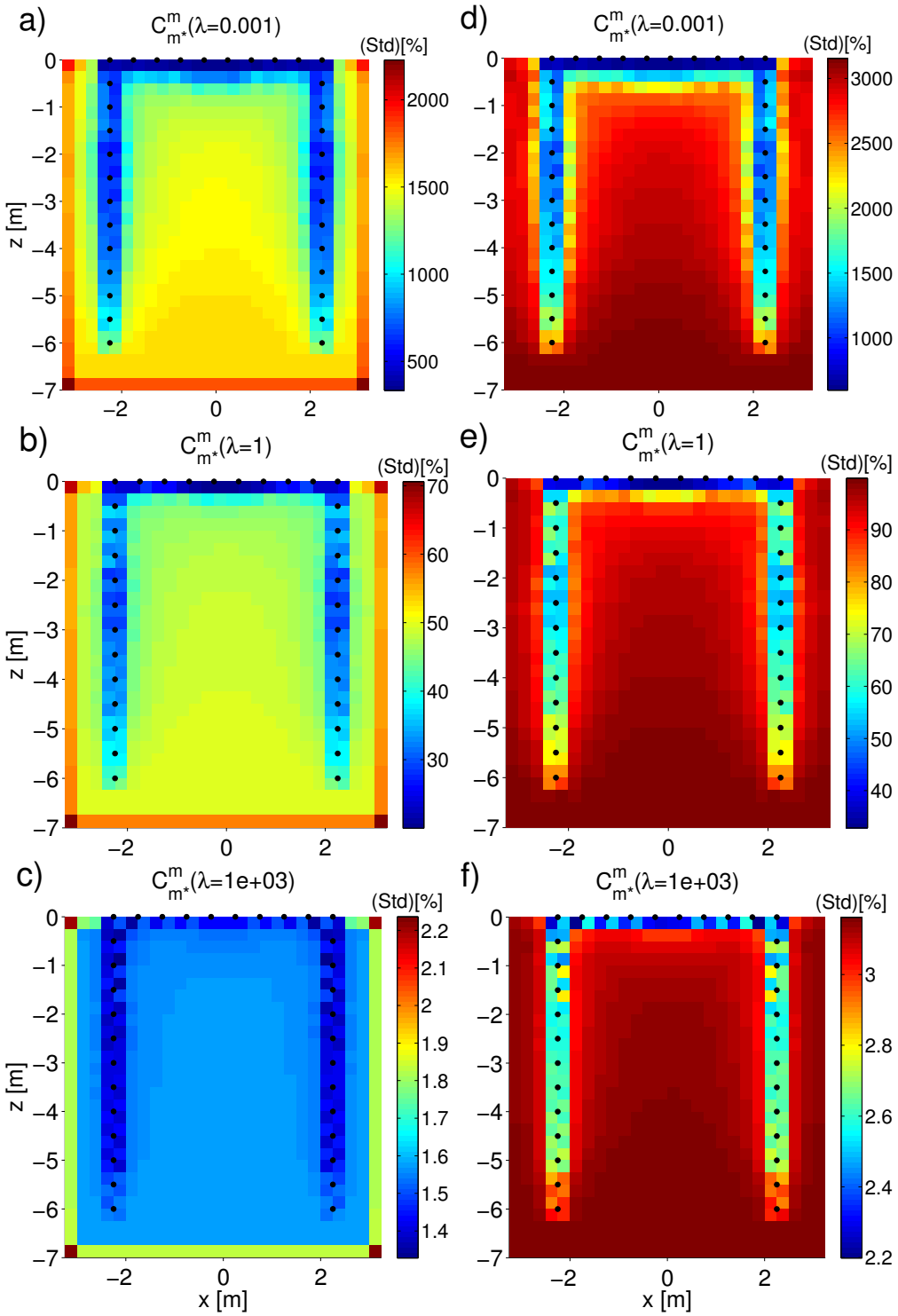

Figure 8: Results of linear uncertainty computation using different regularization means and strength. Pictures to the left (a-c) are computed using smooth regularization and (d-f) is obtained using damping. Also we varied the regularization strength by increasing the regularization parameter λ from $1e-3$ (vanishing regularization) to $1e+3$ (strong regularization), which is also indicated by each subfigure title.

hibit a Gaussian shape and thus reveal the statistics of the input random ensembles (Figs. 6 a,b).

Quantitatively, the model uncertainties caused by prior model uncertainty are larger than the ones due to propagation of data errors, at least for the ranges of data noise considered in our studies. This suggests that the former should be used in practice to avoid underestimation of parameter uncertainty. The Monte Carlo results indicate the limitations of the linear schemes for model uncertainty prediction: The values for prior model and data error propagation are not only in the same range, which is not for the linear approach, but also reveal the degree of non-linearity of the problem. However, the values for the linear posteriori variance computation (eq. 25) and the ones computed with the non-linear approach are comparable for appropriate regularization parameter (optimal regularization parameter for the OCCAM-OE: $\lambda = 260$).

References

Alumbaugh, D. L., 2000. Linearized and nonlinear parameter variance estimation for two-dimensional electromagnetic induction inversion, *Inverse Problems*, **16**(5), 1323.

Alumbaugh, D. L. & Newman, G. A., 2000. Image appraisal for 2-D and 3-D electromagnetic inversion, *Geophysics*, **65**, 1455–1467.

Backus, G. & Gilbert, F., 1968. The resolving power of gross earth data, *Geophysical Journal of the Royal Astronomical Society*, **16**(2), 169–205.

Binley, A. & Kemna, A., 2005. *Hydrogeophysics*, chap. DC resistivity and induced polarization methods, pp. 129–156, Springer.

Constable, S. C., Parker, R. L., & Constable, C. G., 1987. Occam's inversion: a practical algorithm for generating smooth models from em sounding data, *Geophysics*, **52**, 289–300.

Flores Orozco, A., Williams, K. H., Long, P. E., Hubbard, S. S., & Kemna, A., 2011. Using complex resistivity imaging to infer biogeochemical processes associated with bioremediation of an uranium-contaminated aquifer, *J. Geophys. Res.*, **116**(G3), G03001–.

Gubbins, D., 2004. *Time series analysis and inverse theory for geophysicists*, Cambridge Univ. Press.

Kemna, A., 2000. *Tomographic inversion of complex resistivity - theory and application*, Ph.D. thesis, Ruhr-Universität Bochum.

Marquardt, D., 1963. An algorithm for least squares estimation of non-linear parameters, *SIAM J. Sci. Stat. Comput.*, **11**, 431–441.

Menke, W., 1984. *Geophysical data analysis: discrete inverse theory*, Academic Press inc.

Oldenburg, D. & Li, Y., 2005. *Near surface geophysics*, chap. Inversion for applied geophysics, pp. 89–150, Soc. Exp. Geophys.

Slater, L., Binley, A., Daily, W., & Johnson, R., 2000. Cross-hole electrical imaging of a controlled saline tracer injection, *Journal of Applied Geophysics*, **44**(2-3), 85 – 102.

Tarantola, A., 1987. *Inverse problem theory, methods for data fitting and model parameter estimation*, Elsevier, Amsterdam.

Tikhonov, A. N. & Arsenin, V. A., 1977. *Solution of Ill-posed Problems*, Winston & Sons, Washington.